Molecular Therapy
Nucleic Acids
Original Article

Circular RNA Profiling Reveals Exosomal circ_0006156 as a Novel Biomarker in Papillary Thyroid Cancer

Guojun Wu,[1,2,5] Wenhong Zhou,[3,5] Xiaohua Pan,[1] Zhigang Sun,[1] Yongjie Sun,[2] Hao Xu,[1] Peng Shi,[1] Jiyu Li,[1] Ling Gao,[4] and Xingsong Tian[1]

[1]Department of Breast and Thyroid Surgery, Shandong Provincial Hospital Affiliated to Shandong University, Jinan 250021, China; [2]Department of Breast and Thyroid Surgery, Shandong Provincial ENT Hospital Affiliated to Shandong University, Jinan 250022, China; [3]Department of Nursing, Shandong Provincial Hospital Affiliated to Shandong University, Jinan 250021, China; [4]Scientific Center, Shandong Provincial Hospital Affiliated to Shandong University, Jinan 250021, China

Circular RNAs (circRNAs) are a class of noncoding RNAs that are broadly expressed in various biological cells and function in regulating gene expression. However, the molecular mechanisms that link circRNAs with progression of papillary thyroid carcinoma (PTC) are not well understood. In the present study, the function of circ_0006156 (circFNDC3B) was investigated in human PTC cells. First, we detected the expression of circFNDC3B in PTC tissues and PTC cell lines by RT-PCR. A luciferase reporter assay and AGO2-RNA immunoprecipitation (RIP) was used to confirm the relationship between circFNDC3B and microRNA (miR)-1178. PTC cells were stably transfected with small interfering RNA (siRNA) against circFNDC3B, and cell proliferation, migration, and invasion were detected to evaluate the effect of circFNDC3B in PTC, while tumorigenesis was assayed in nude mice. In this study, circFNDC3B was observed to be upregulated in PTC tissues and cell lines. Knockdown of circFNDC3B inhibited cell proliferation and promoted cell apoptosis in PTC cells. Bioinformatics analysis predicted that there is a circFNDC3B/miR-1178/Toll-like receptor 4 (TLR4) axis in PTC. The dual-luciferase reporter system validated the direct interaction of circFNDC3B, miR-1178, and TLR4. Furthermore, circFNDC3B facilitates PTC progression *in vivo*. Importantly, we demonstrated that circFNDC3B was upregulated in serum exosomes from PTC patients. In summary, our study demonstrated that circFNDC3B modulates PTC progression through the miR-1178/TLR4 pathway. Our findings indicated that circFNDC3B may serve as a promising therapeutic target for the treatment of PTC patients.

INTRODUCTION

Thyroid cancer (TC) is the most common endocrine-related malignancy; it has a continuously increasing incidence and has attracted much attention from the public for several decades.[1] The most common type of thyroid cancer is papillary thyroid carcinoma (PTC), which accounts for close to 85% of all thyroid cancer.[2] Most patients with PTC can be cured by traditional clinical managements, such as thyroidectomy, radioiodine, or thyroid-stimulating hormone (TSH) suppression therapy. Although the 5-year overall survival rate of PTC patients is about 95%, tumors can metastasize into distant organs and lymph nodes, resulting in poor prognosis and high reoccurrence in some patients.[3,4] Therefore, it is essential to explore a novel method for diagnosis and treatment.

Circular RNAs (circRNAs) are a group of transcripts characterized by a covalently closed loop structure without polarities and polyadenylated tails.[5,6] Studies have highlighted important roles of circRNAs in both physiological and pathological settings, such as cellular metabolism and almost all types of cancers.[7,8] Various circRNAs have been identified as cancer-related circRNAs in the tumorigenesis.[9,10] Multiple circRNAs, such as circZFR, circ-ITCH, and circFNDC3B, are reported to play crucial roles in thyroid cancer.[11–13] circ_0006156 (circFNDC3B) is a circRNA shears from fibronectin type III domain-containing protein 3B (FNDC3B), which has been presented to play a promoting or restraining efficacy in carcinoma. For instance, Liu et al.[14] reflected that circFNDC3B restrains bladder carcinoma, whereas Hong et al.[15] reflected that circFNDC3B enhances gastric carcinoma. The expression of circFNDC3B is uncertain in diverse cells. However, there were few studies on circFNDC3B, and the efficacy of circFNDC3B in PTC has not been reported.

Exosomes are generated inside multivesicular endosomes and can be secreted from multiple types of cells and participate in intercellular communication by transmitting intracellular cargoes, such as proteins and nucleic acids.[16] It has been reported that numerous circRNAs could be transferred between cancer cells via exosomes.[17]

Received 25 July 2019; accepted 20 December 2019;
https://doi.org/10.1016/j.omtn.2019.12.025.

[5]These authors contributed equally to this work.

Correspondence: Xingsong Tian, Department of Breast and Thyroid Surgery, Shandong Provincial Hospital Affiliated with Shandong University, Jinan 250021, Shandong, China.
E-mail: xingsong_tianxs@sina.cn
Correspondence: Ling Gao, Scientific Center, Shandong Provincial Hospital Affiliated with Shandong University, Jinan 250021, Shandong, China.
E-mail: gaoling8822@sina.com

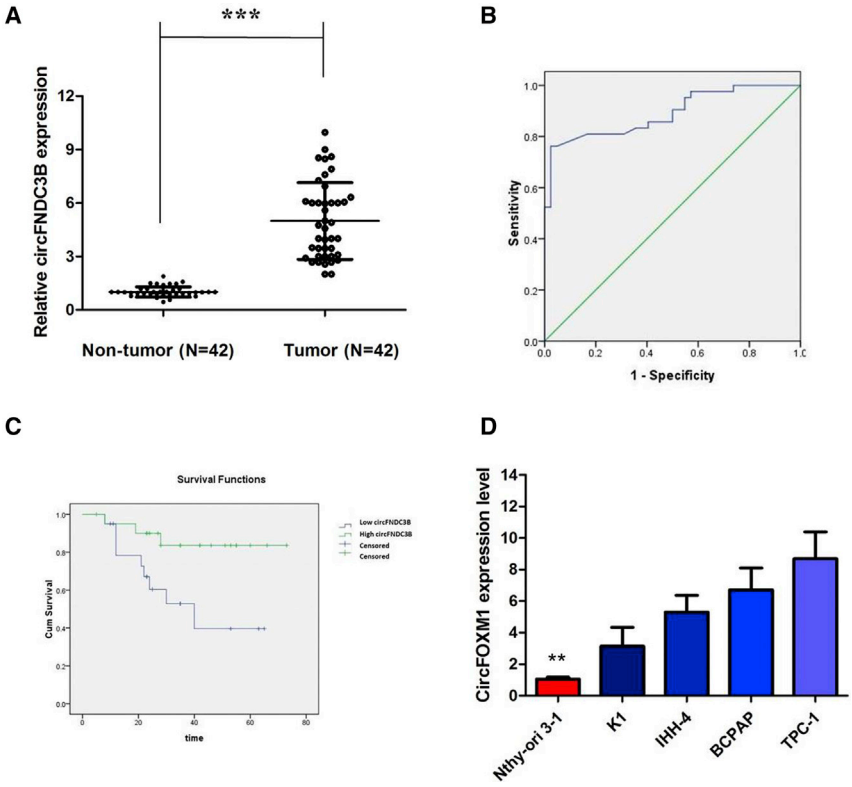

Figure 1. circFNDC3B Is Highly Expressed in PTC Tissues and PTC Cell Lines

(A) circFNDC3B levels were detected by RT-PCR in PTC tissues (n = 42) compared with paratumor tissue samples (n = 42). (B) The area under the ROC curve was 0.891 (95% CI = 0.820–0.961, $p < 0.0001$). (C) Kaplan-Meier survival curve of patients with low and high expression of circFNDC3B. (D) circFNDC3B expression levels in PTC cell lines and human thyroid follicular epithelial cells were analyzed by RT-PCR. Data indicate the mean ± SD, n = 3. $^{**}p < 0.01$, $^{***}p < 0.001$ versus control.

RNA sequencing data showed that the concentration of circRNA in exosomes was greater than in normal cells,[18,19] and a further study has indicated that exosome circRNAs could reflect circRNA levels in cells and tissues.[20] However, the roles and functions of exosomes, specifically exosomal circRNAs derived from PTC cells, are still unknown.

In this study, we demonstrated that circFNDC3B was markedly upregulated in PTC tissues and cell lines. By analyzing the relationship between circFNDC3B and clinicopathological characteristics, we found that tumor size, lymph node metastasis, extrathyroidal extension, and advanced tumor-node-metastasis (TNM) stage were related to the high expression of circFNDC3B. Loss-of-function assays indicated that circFNDC3B promoted cell proliferation, migration, and invasion and reduced apoptosis *in vitro*. Bioinformatics analysis, together with biological experiments, was performed to verify the underlying mechanism by which circFNDC3B exerted its malignant properties. In short, circFNDC3B acts as a competing endogenous RNA (ceRNA) to sponge microRNA (miR)-1178 and then regulate Toll-like receptor 4 (TLR4) in PTC, suggesting that it can be a target for diagnosis and therapy.

RESULTS

circFNDC3B Is Highly Expressed in PTC Tissues and PTC Cell Lines

First, in order to investigate the relationship between circRNA and PTC, we analyzed the online dataset (GEO: GSE93522). According to this data, we found that circRNA_0006156 is one of the upregulated circRNAs in PTC tissues compared to normal control tissues. Thus, we chose it to further investigation. circFNDC3B (hsa_circ_0006156) is derived from exon 5 and exon 6 of the FNDC3B gene, whose spliced mature sequence length is 526 bp. This gene is located on chromosome 3:171965322-171969331. We examined the expression level of circFNDC3B in PTC tissues and cell lines. We found that circFNDC3B is highly expressed in 42 PTC tissues compared with matched paratumor tissues (Figure 1A). We used the receiver operating characteristic (ROC) curve to examine the diagnostic value of circFNDC3B in PTC tissues compared with paratumor tissues and found the area under the ROC curve (AUC) to be 0.891 (95% confidence interval [CI] = 0.820–0.961, $p < 0.0001$; Figure 1B). Then, the correlations of circFNDC3B expression and special clinicopathological parameters and prognosis of PTC were analyzed, as shown in Table 1. Furthermore, PTC patients with low expression of circFNDC3B displayed obviously longer overall survival times than those with high expression of circFNDC3B, according to the Kaplan-Meier survival curve analysis ($p < 0.05$; Figure 1C).

Similarly, a high degree of circFNDC3B upregulation was observed in all PTC cell lines compared with that in Nthy-ori 3-1 (Figure 1D). Because the circFNDC3B level was the highest in TPC-1 cells, whereas K1 cells exhibited the relative lowest expression level of circFNDC3B, we knocked circFNDC3B down in the TPC-1 cell lines using specific small interfering RNAs (siRNAs), whereas K1 cells were selected for the following circFNDC3B gain-of-function assay (Figures 2A and 2B). The levels of FNDC3B did not change when the expression of circFNDC3B was artificially changed in PTC cells (Figures 2C and 2D), indicating that FNDC3B is not the target gene of circFNDC3B.

Confirmation of Subcellular Localization of circFNDC3B

We investigated the stability and localization of circFNDC3B in TPC-1 cells. Total RNAs from TPC-1 cells were isolated at the indicated time points after treatment with actinomycin D, an inhibitor of

Table 1. Clinical Characteristics of PTC Patients According to circFNDC3B Expression Levels

	circFNDC3B Expression		
	Low	High	
Characteristics	(n = 21)	(n = 21)	p Value
Age, Year			
≥45	11	16	0.197
Gender			
Female	10	15	0.208
Tumor Size			
>1	4	15	0.001
Lymph Node Metastasis			
Yes	6	14	0.029
TNM Stage Group			
II–IV	6	15	0.012
Multifocality			
Yes	5	9	0.326

transcription. Analysis for stability of circFNDC3B and FNDC3B in TPC-1 cells treated with actinomycin D, an inhibitor of transcription, revealed that the half-life of the circFNDC3B transcript exceeded 24 h, with more stability than FNDC3B (Figure 3A). Furthermore, we found that circFNDC3B was resistant to RNase R digestion (Figure 3B). These data confirmed that circFNDC3B was a circular RNA. We then investigated the localization of circFNDC3B. qRT-PCR of RNAs from nuclear and cytoplasmic fractions indicated that circFNDC3B was predominantly localized in the cytoplasm of TPC-1 cells (Figure 3C). Collectively, the above data suggested that circFNDC3B harbored a loop structure and was predominantly localized in the cytoplasm.

Silenced circFNDC3B Expression Inhibits PTC Cell Proliferation, Migration, and Invasion and Promotes Cell Apoptosis

Cell Counting Kit-8 (CCK8) and colony formation assays were performed to examine the proliferative ability of TPC-1 cells after circFNDC3B silencing. The results of CCK8 and colony formation assays showed that the inhibition of circFNDC3B expression clearly decreased the proliferation of TPC-1 cells (Figures 3D and 3F), whereas overexpression of circFNDC3B efficiently enhanced cell viability and proliferation of K1 ($p < 0.01$; Figures 3E and 3G).

Knockdown of circFNDC3B caused significant G1-phase cell-cycle arrest of TPC-1 cells ($p < 0.01$; Figure 3H). Enhanced circFNDC3B expression increased the S-phase percentage and decreased the G0/G1-phase percentage of K1 cells ($p < 0.01$; Figure 3I). Furthermore, flow cytometry analysis revealed that the proportion of apoptotic TPC-1 cells after depletion of circFNDC3B was apparently increased, whereas overexpression of circFNDC3B decreased the proportion of apoptotic K1 cells (Figures 4A and 4B). In addition, *in vitro* cell migration and invasion assays were employed to analyze the effect of circFNDC3B knockdown on the migration and invasion of PTC cells. The results showed that knocking down circFNDC3B expression substantially attenuated the migration and invasion of TPC-1 cells (Figure 4C), whereas overexpression of circFNDC3B promoted the ability of cell migration and invasion of K1 cells (Figure 4D). These observations collectively identified the pro-oncogenic actions of circFNDC3B in the PTC progression.

circFNDC3B Knockdown Inhibits the Growth of PTC Cells *In Vivo*

Finally, an *in vivo* tumorigenicity assay was conducted to analyze the role of circFNDC3B in tumor growth of PTC cells *in vivo*. The tumor xenografts in the circFNDC3B-specific short hairpin RNA (shRNA; sh-circFNDC3B) group developed smaller tumor volumes (Figure 5A) and lighter tumor weights (Figure 5B) relative to those in the negative control shRNA (sh-NC) group. After removing the tumor xenografts, quantitative real-time PCR (qRT-PCR) analysis was performed to detect circFNDC3B expressions. Lower circFNDC3B levels (Figure 5C) were observed in the tumor xenografts derived from sh-circFNDC3B-transfected TPC-1 cells. Immunohistochemistry (IHC) staining results showed that knockdown of circFNDC3B significantly inhibited the expression levels of Ki-67 when compared with the control group (Figure 5D). In a word, a reduction in circFNDC3B expression impaired tumor growth of PTC cells *in vivo*.

circFNDC3B Acts as a Molecular Sponge for miR-1178-3p in PTC Cells

circRNAs exert their functions via different working mechanisms, including ceRNA. To identify the potential mechanism via which circFNDC3B modulates the oncogenicity of PTC, we detected the intracellular location of circFNDC3B and found that this circRNA was predominantly localized in the cytoplasm, which indicates that circFNDC3B may perform its roles in PTC progression by acting as a ceRNA for certain microRNA (miRNA). To test this hypothesis, bioinformatics analysis was performed to predict the miRNAs that could interact with circFNDC3B (Table S1). The analysis indicated that 21 potential miRNAs that could bind to circFNDC3B and miR-1178 share complementary binding sequences with circFNDC3B (Figure 6A). A subsequent luciferase reporter assay revealed that the luciferase intensity was reduced after the cotransfection of the wild-type (WT) luciferase reporter and miR-1178 mimics, whereas the mutated luciferase reporter exerted no such effect ($p < 0.01$; Figure 6B). In a further RNA immunoprecipitation (RIP) experiment, circFNDC3B and miR-1178 simultaneously existed in the production precipitated by anti-argonaute 2 (AGO2) ($p < 0.01$; Figure 6C), which indicates that circFNDC3B directly interacts with miR-1178 and could act as a sponge for miR-1178.

TLR4 Was a Direct Target of miR-1178

To validate whether circFNDC3B sponges miR-1178 and liberates the expression of its downstream target, we searched TargetScan for potential target genes of miR-1178, and TLR4 was predicted (Figure 6D). A subsequent luciferase reporter assay revealed decreased luciferase intensity after cotransfection of miR-1178 mimics and the wild-type luciferase reporter, whereas the mutated luciferase reporter

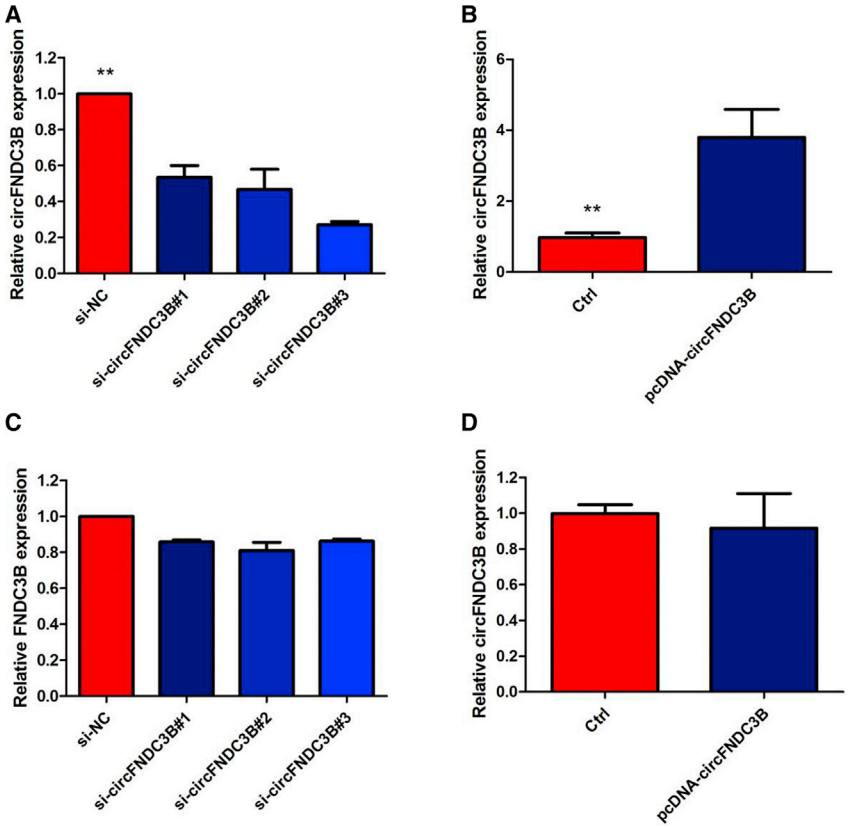

Figure 2. Inhibition of circFNDC3B in the TPC-1 Cell Line and Overexpression of circFNDC3B in the K1 Cell Line

(A) The qRT-PCR assay indicated the relative abundance of circFNDC3B in TPC-1 cells treated with si-circFNDC3B. (B) The qRT-PCR assay indicated the relative abundance of circFNDC3B in K1 cells infected with circFNDC3B overexpression plasmid. (C) The qRT-PCR assay indicated the relative abundance of FNDC3B in TPC-1 cells treated with si-circFNDC3B. (D) The qRT-PCR assay indicated the relative abundance of FNDC3B in K1 cells infected with circFNDC3B overexpression plasmid. Data indicate the mean ± SD, n = 3. **p < 0.01 versus control.

exerted no such effect (Figure 6E). The results of qRT-PCR showed that TLR4 expression in PTC specimens was significantly upregulated compared with that in the adjacent normal tissues (< 0.001; Figure 6F). Furthermore, we investigated whether TLR4 expression can be modulated by circFNDC3B. The results of qRT-PCR and western blotting showed that the expression of TLR4 was decreased by circFNDC3B silencing in TPC-1 at both mRNA and protein levels, while a miR-1178 inhibitor attenuated the effect of inhibition of circFNDC3B (Figures 6G and 6H). These data further demonstrated the regulatory network of circFNDC3B/miR-1178/TLR4.

circFNDC3B Is Secreted by Exosomes into Serum of PTC Patients

Finally, in our current study, we collected an abundancy of serums from 42 PTC patients and 40 healthy donors. After isolation of serum exosomes by sequential centrifugation, transmission electron microscopy (TEM) analysis showed that isolated, PTC-secreted exosomes had similar morphologies (30–150 nm in diameter) and exhibited a round-shaped appearance (Figure 7A). The nanoparticle tracking analysis (NTA) results demonstrated that isolated PTC-secreted exosomes showed a similar size distribution, and the peak size range was 80–135 nm. Moreover, the presence of the exosome markers CD63, TSG101, and heat shock protein (HSP)70 was confirmed by western blot (Figure 7B). Our results showed that circFNDC3B expression is detectable in extracted serum exosomes derived from PTC patients ($p < 0.01$; Figure 7C). Furthermore, there was a significant inverse correlation between the expression levels of circFNDC3B and miR-1178 in serum exosomes derived from PTC patients ($r = -0.470$, $p = 0.0017$; Figure 7D).

DISCUSSION

Increasing evidence showed that circRNA plays critical roles in PTC carcinogenesis. For example, Wang et al.[21] found that circ_0067934 could improve the development of thyroid carcinoma by promoting epithelial-to-mesenchymal transition (EMT) and phosphatidylinositol 3-kinase (PI3K)/protein kinase B (AKT) signaling pathways. Pan et al.[22] uncovered a novel signal of circ_0025033/miR-1231/miR-1304 involved in PTC initiation and progression. Liu et al.[23] reported that circular RNA EIF6 (hsa_circ_0060060) sponges miR-144-3p to promote the cisplatin resistance of human thyroid carcinoma cells by autophagy regulation. Recently, circFNDC3B has been demonstrated to be participants in various biological processes by different mechanisms. circFNDC3B is produced by FNDC3B located on chr3. For example, Garikipati et al.[24] found that provide evidence that overexpression of circFNDC3b in ischemic hearts can reduce cardiomyocyte apoptosis, enhance angiogenesis, and attenuate left ventricular (LV) dysfunction post-myocardial infarction (MI) in mice. Mechanistically, we provide evidence that circFNDC3b enhances vascular endothelial growth factor-A (VEGF-A) expression and signaling via its interaction with the RNA binding protein fused in sarcoma (FUS)[24]. Hong et al.[15] found that when circFNDC3B was upregulated, it promoted cell migration and invasion of gastric cancer cells via the formation of a ternary complex of circFNDC3B-IGF2BP3-CD44 mRNA and the modulation of E-cadherin in gastric cancer. However, Liu et al.[14] found that invasion-related circular RNA circFNDC3B inhibits bladder cancer progression through the miR-1178-3p/G3BP2/SRC/FAK axis. Nonetheless, the oncogenic or tumor-suppressive role of circFNDC3B in PTC remains to be demonstrated.

In this present study, we thoroughly investigated the expression, biological roles, and mechanisms of action of circFNDC3B in PTC. We

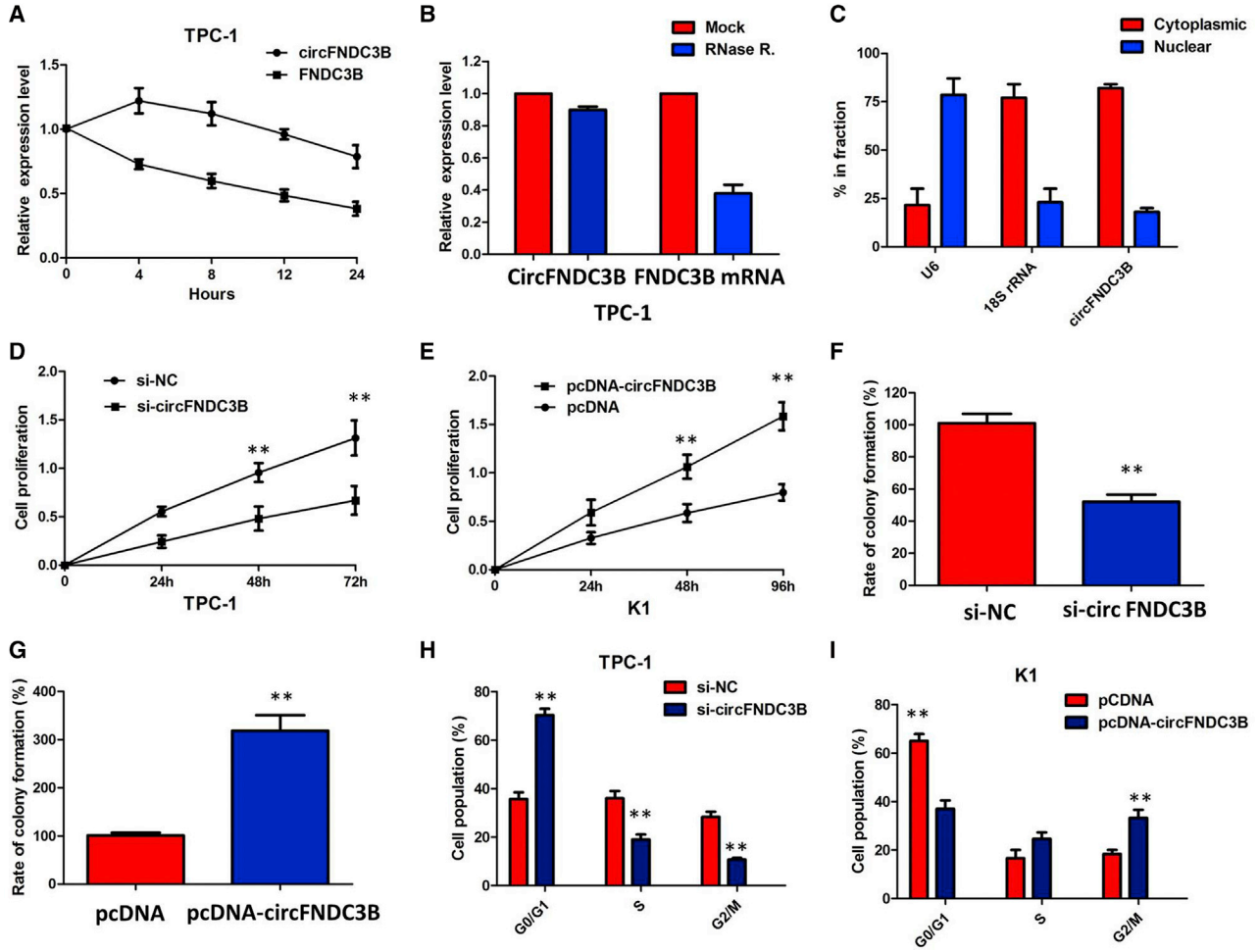

Figure 3. Confirmation of Subcellular Localization of circFNDC3B

(A) qRT-PCR for the abundance of circFNDC3B and FNDC3B in TPC-1 cells treated with actinomycin D at the indicated time point. The error bars represent SD (n = 3). (B) qRT-PCR for the expression of circFNDC3B and FNDC3B mRNA in TPC-1 cells treated with or without RNase R. The results indicated that circFNDC3B was resistant to RNase R digestion. (C) Levels of circFNDC3B in the nuclear and cytoplasmic fractions of TPC-1 cells. The results showed that circFNDC3B was predominantly localized in the cytoplasm. (D) The CCK8 assay showed that circFNDC3B knockdown significantly repressed cell proliferation of TPC-1 cells. (E) The CCK8 assay showing overexpression of circFNDC3B promoted the proliferation of K1 cells. (F) Colony-formation assay showed that the knockdown of circFNDC3B significantly restrained the proliferation of TPC-1 cells. (G) Colony-formation assay showed that the ectopic expression of circFNDC3B significantly promoted the proliferation of K1 cells. (H) The flow cytometry analysis showed that circFNDC3B knockdown led to an arrest in the G1 phase of TPC-1 cells. (I) The flow cytometry analysis showed that overexpression of circFNDC3B decreased the G0/G1-phase percentage of K1 cells. Data are listed as mean ± SD of at least three independent experiments. $^{**}p < 0.01$.

found that circFNDC3B was significantly elevated in PTC tissues and cell lines compared with normal tissues and the Nthy-ori 3-1 cell line. Elevated expression of circFNDC3B was positively correlated with tumor size, tumor stage, and poor lymph node metastasis. Gain-of-function experiments revealed that ectopic expression of circFNDC3B promoted proliferation and inhibited apoptosis of PTC cells. Loss-of-function experiments revealed that knockdown of circFNDC3B inhibited proliferation and promoted apoptosis of PTC cells. In addition, xenograft experiments showed that circFNDC3B promoted PTC xenograft growth *in vivo*. Specifically, we also showed mechanistically that circFNDC3B promotes the progression of PTC by acting as the sponge of miR-1178. Finally, we showed that overexpressed circFNDC3B was secreted by exosomes into the serum of PTC patients, suggesting that circFNDC3B might be a novel, clinical molecular marker for PTC patients.

Functionally, upregulated circRNAs can promote cell proliferation and inhibit apoptosis, thereby facilitating tumorigenesis.[25–27] In our current study, we investigated whether circFNDC3B was a regulator in tumorigenesis of PTC. Both gain- or loss-of function assays were carried out in two PTC cell lines. As expected, high expression of circFNDC3B promoted cell proliferation and suppressed cell apoptosis, indicating the oncogenic property of circFNDC3B in PTC cells. *In vivo* animal study further demonstrated that

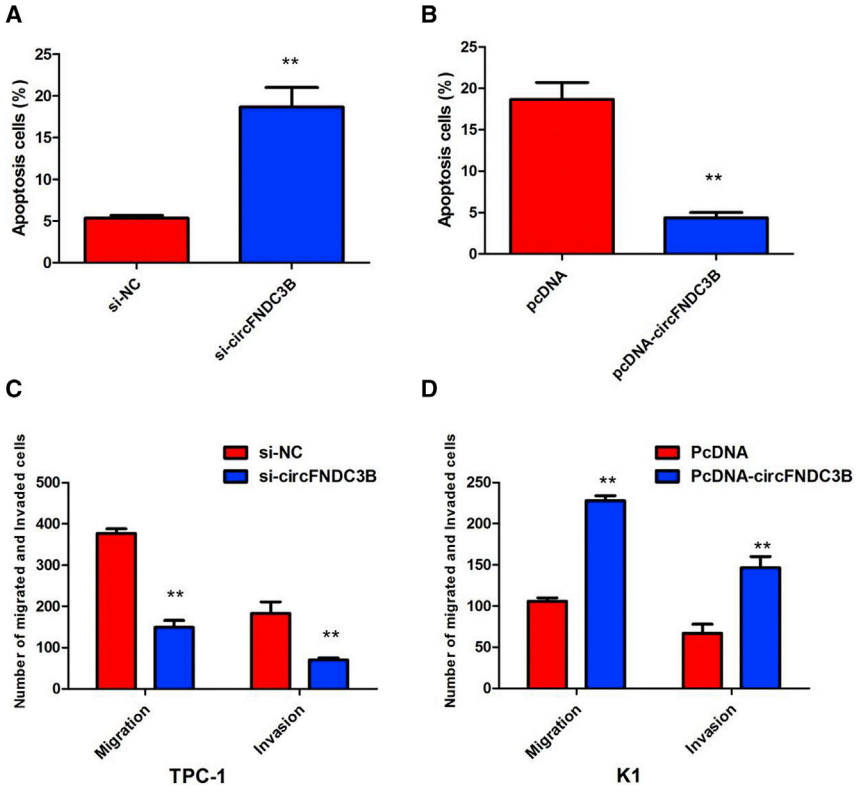

Figure 4. Silenced circFNDC3B Expression Inhibits PTC Cell Migration, and Invasion and Promotes Cell Apoptosis

(A) The flow cytometry analysis showed that circFNDC3B knockdown increased the proportion of apoptotic TPC-1 cells. (B) The flow cytometry analysis showed that overexpression of circFNDC3B decreased the proportion of apoptotic K1 cells. (C) Cell migration and invasion assays showed that circFNDC3B knockdown substantially attenuated the migration and invasion of TPC-1 cells. (D) Cell migration and invasion assays showed that overexpression of circFNDC3B promoted the ability of cell migration and invasion of K1 cells. Data are listed as mean ± SD of at least three independent experiments. $^{**}p < 0.01$.

circFNDC3B could promote PTC growth. These data indicated that circFNDC3B exerted oncogenic function in the tumorigenesis of PTC.

In recent years, emerging evidence proposed that circRNAs are an important subtype of ceRNAs, and circRNA can be used as a miRNA molecular sponge to attenuate the effect of miRNAs on gene expression by combining with miRNA response elements (MREs).[28–30] We used the StarBase v2.0 target prediction tool to find 21 potential miRNAs that could bind to circFNDC3B. Accordingly, we performed the RIP and luciferase assays and found that the mechanism by which circFNDC3B promotes tumor progression of PTC *in vitro* is mediated by inhibiting miR-1178 expression. Moreover, miRNAs are the most widely studied noncoding RNAs and also can act as oncogenes or tumor-suppressor genes.[31] In this study, bioinformatics analysis showed that miR-1178 interacted with the 3′ UTR of TLR4 and suppressed TLR4 expression at the post-transcriptional level, which was confirmed by the results of the luciferase reporter assay. The expression of TLR4 was decreased by circFNDC3B silencing in TPC-1 at both mRNA and protein levels, while a miR-1178 inhibitor attenuated the effect of inhibition of circFNDC3B. Taken together, these findings indicate that circFNDC3B can exert function in PTC by sponging miR-1178 to upregulate TLR4 expression.

Exosomes have been reported to be involved in each process of cancer, such as angiogenesis, metastasis, EMT, and immune escape.[32]

Although several studies have shown that exosomal circRNAs are potential markers for cancer,[20] none are aimed at clarifying the expression of cancer-secreted circRNAs in PTC. Here, we performed TEM to reveal the shapes and size of exosomes from plasma of PTC patients. Notably, we found that the highly expressed circFNDC3B could be examined to serum exosomes of PTC patients.

Above all, our present study demonstrated that circFNDC3B was upregulated in PTC tissues and cell lines and was an oncogenic factor that promoted tumorigenesis. circFNDC3B acted as a ceRNA of miR-1178 and released TLR4 to promote the development of PTC, which might well aid in intervention strategies of PTC in the future. Thus, our data enhance our understanding of circRNA biology and may assist in the development of additional biomarkers or more effective therapeutic targets for PTC.

MATERIALS AND METHODS

Clinical Samples

The paired samples used in this study (n = 42), consisting of tumor tissue and adjacent unaffected thyroid tissue from PTC patients collected at the Department of Breast and Thyroid Surgery, Shandong Provincial Hospital Affiliated to Shandong University, from January 2010 to January 2018, were collected. All cases were confirmed via pathological diagnosis. These patients did not receive the chemotherapy, radiotherapy, or other treatments of thyroid cancer before operation. All of the patients were pathologically confirmed, and the tissues were collected immediately after they were obtained during the surgical operation and then stored at −80°C to prevent RNA loss. For exosome purification, serum samples were collected from these 42 cases of PTC and 40 cases of healthy donors. All patients provided written, informed consent in accordance with the Declaration of Helsinki. The procedures in the study were scrutinized and approved by the Medical Ethics Committee of Shandong Provincial Hospital Affiliated to Shandong University.

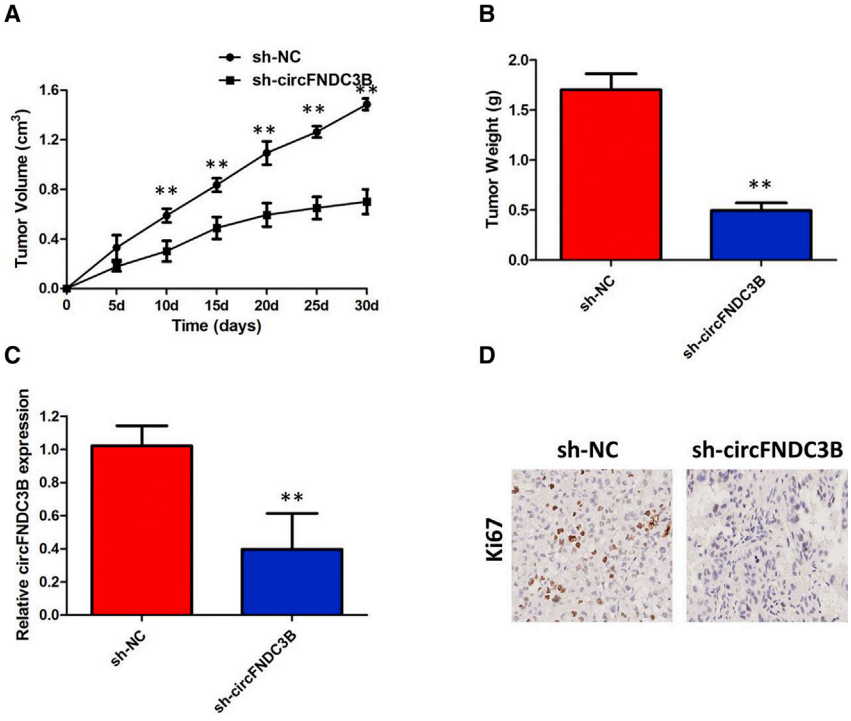

Figure 5. circFNDC3B Knockdown Inhibits the Growth of PTC Cells *In Vivo*

(A) circFNDC3B knockdown inhibits tumor growth *in vivo*. The tumor volume curve of nude mice was analyzed. (B) The tumor weights of nude mice were measured. (C) qRT-PCR analysis was performed to detect circFNDC3B expressions. (D) IHC analysis was performed to examine the expression levels of proliferation marker Ki-67 in tumors of nude mice. **$p < 0.01$.

Cell Culture and Transfection

Human PTC cell lines K1, IHH-4, BCPAP, and TPC-1 and human thyroid follicular epithelial cells Nthy-ori 3-1 were obtained from the Shanghai Institute of Cell Biology (Shanghai, China) and were cultured in RPMI-1640 medium (HyClone, Logan, UT, USA) with 10% fetal bovine serum (FBS) and 1% antibiotics (both from Gibco-BRL, Gaithersburg, MD, USA). Oligonucleotide transfection siRNA, miRNA mimics, and inhibitors were purified and synthesized by RiboBio (Guangzhou, China) or Gene-Pharma (Shanghai, China). The lentivirus targeting human circFNDC3B was purchased from GeneChem (Shanghai, China). Transfection was performed using the Lipofectamine 2000 reagent (Invitrogen). The circFNDC3B sequences were subcloned into pGLV3/H1/GFP/Puro vectors to construct sh-circFNDC3B for animal studies.

RNA Extraction and qRT-PCR

The total RNA was isolated from tissues and cell lines using TRIzol reagent (Invitrogen, CA, USA), and exosomal RNA was extracted from plasma and culture medium using the exoRNeasy Midi Kit (QIAGEN, Valencia, CA, USA), according to the manufacturer's protocol. For circRNAs, RNase R was used to degrade linear RNAs, which have poly (A), and amplified by a divergent primer. Specific divergent primers spanning the back-splice junction site of circRNAs were designed. To quantify the amount of mRNA and circRNA, cDNA was synthesized using PrimeScript RT Reagent Kit (TaKaRa, Dalian, China). The qRT-PCR analysis on circular RNA and mRNA was performed using Prime Script RT Reagent Kit (TaKaRa) and SYBR Premix Ex Taq II (TaKaRa). β-Actin was used as an endogenous control. For miR-1178 analysis, miRNA was treated with DNase I to eliminate genomic DNA, and cDNA was synthesized by Mir-X miR First-Strand Synthesis Kit (TaKaRa). SYBR Premix Ex Taq II (TaKaRa) was used for qRT-PCR. The expression was normalized to RNU6-2. The $2^{-\Delta\Delta CT}$ method was adopted to calculate relative expression.

Actinomycin D and RNase R Treatment

To block transcription, 2 mg/mL actinomycin D or dimethyl sulfoxide (Sigma-Aldrich, St. Louis, MO, USA) as a negative control was added into the cell culture medium. For RNase R treatment, total RNA (2 μg) was incubated for 30 min at 37°C, with or without 3 U/μg of RNase R (Epicenter Technologies, Madison, WI, USA). After treatment with actinomycin D and RNase R, qRT-PCR was performed to determine the expression levels of circFNDC3B and FNDC3B mRNA.

Isolating RNAs from Nucleus and Cytoplasmic Fractions

The nuclear and cytoplasmic fractions were isolated using the PARIS Kit (Invitrogen, Carlsbad, CA, USA), following the manufacturer's protocol. Briefly, cells were collected and lysed with cell-fractionation buffer, followed by centrifugation to separate the nuclear and cytoplasmic fractions. The supernatant containing the cytoplasmic fraction was collected and transferred to a fresh RNase-free tube. The nuclear pellet was lysed with cell disruption buffer. The cytoplasmic fraction and nuclear lysate were mixed with 2 times lysis/binding solution and then added with 100% ethanol. The sample mixture was drawn through a filter cartridge, followed by washing with wash solution. The RNAs of nuclear and cytoplasmic fractions were eluted with elution solution. U6 small nuclear RNA (snRNA) and 18S rRNA were employed as positive control for nuclear and cytoplasmic fractions, respectively.

CCK8 Assay

Cells were seeded into 96-well plates, and CCK8 solution (10 μL; Dojindo Laboratories, Japan) was added 48 h after transfection. The absorbance at 450 nM was measured after incubation at 37°C for 2 h with a microtiter plate reader (Epoch 2; BioTek, USA).

Cell Cycle Assay

For cell cycle analysis, transfected cells were fixed in 70% ethanol overnight at −20°C and stained with propidium iodide (Kaiji,

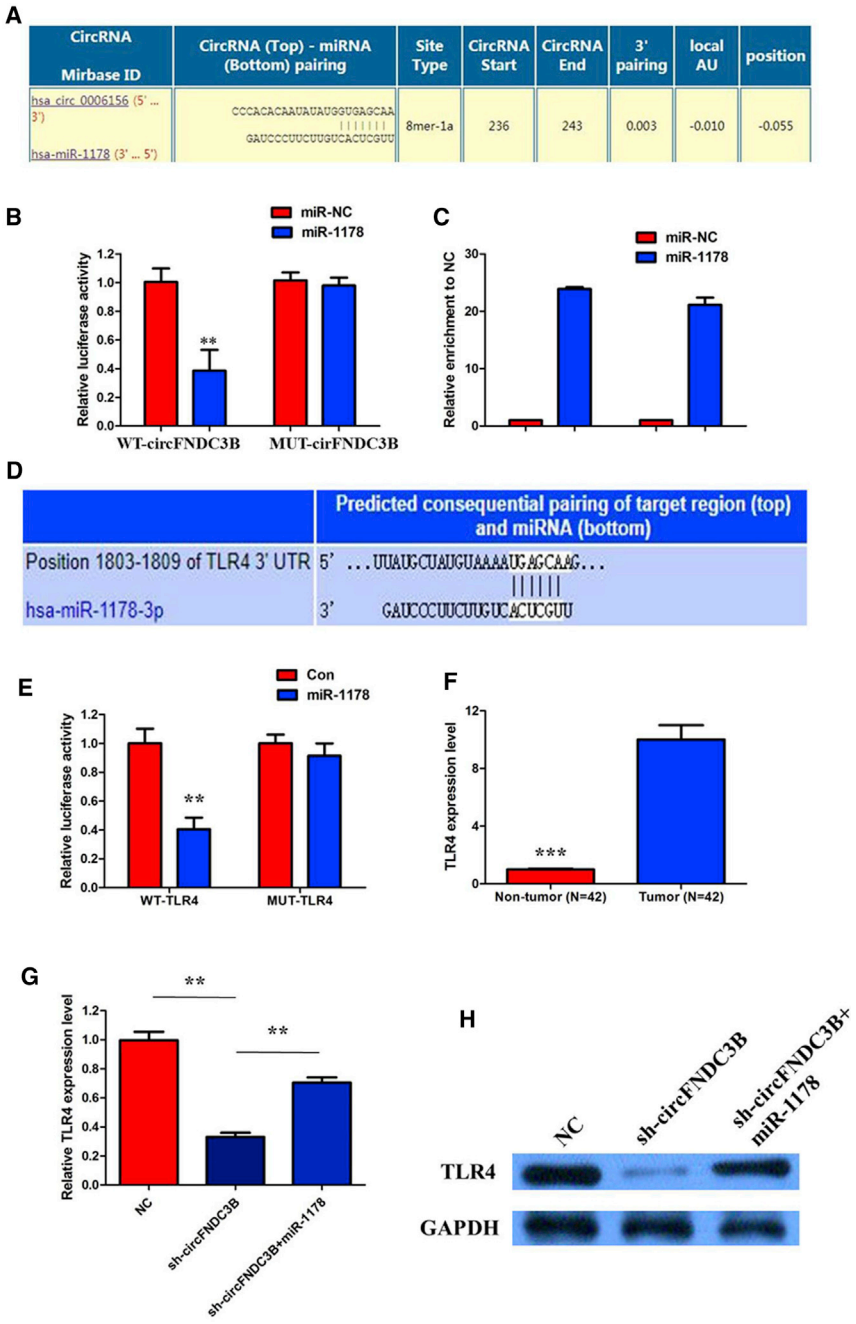

Figure 6. circFNDC3B Acts as a Molecular Sponge for miR-1178-3p in PTC Cells

(A) miR-1178 shares complementary binding sequences with circFNDC3B. (B) The dual-luciferase reporter showed a significant reduction of luciferase activity of the wild-type, and luciferase activity is restored by the mutant sequence. (C) The RIP experiment showed that miR-1178 and circFNDC3B simultaneously existed in the production precipitated by anti-AGO2. (D) Bioinformatics analysis revealed the predicted binding sites between TLR4 and miR-1178. (E) A subsequent luciferase reporter assay revealed decreased luciferase intensity after cotransfection of miR-1178 mimics and wild type luciferase reporter, while the mutated luciferase reporter exerted no such effect; (F) The results of qRT-PCR showed that TLR4 expression in PTC specimens was significantly upregulated compare with that in the adjacent normal tissues; (G) circFNDC3B knockdown could suppress TLR4 mRNA expression, while a miR-1178 inhibitor attenuated the effect of inhibition of circFNDC3B. (H) circFNDC3B knockdown could suppress TLR4 protein expression, while a miR-1179 inhibitor attenuated the effect of inhibition of circFNDC3B. Data are listed as mean ± SD of at least three independent experiments. $^{**}p < 0.01$; $^{***}p < 0.001$.

Nanjing, China). Cell cycle assays were conducted at 48 h after transfection.

Cell Apoptosis Analysis

With the detection of apoptosis by flow cytometry, an Annexin V-allophycocyanin (APC)/4′,6-diamidino-2-phenylindole (DAPI) double-staining kit (Thermo Fisher Scientific) was used to analyze cellular apoptosis. Cells were seeded in 6-well plates (5×10^5 cells/well) and then digested with trypsin (Gibco trypsin-EDTA; Thermo Fisher Scientific), washed with phosphate buffered saline (PBS) three times, suspended in 500 μL of binding buffer, and then incubated with 5 μL of fluorescein isothiocyanate (FITC)-conjugated Annexin V and 3 μL of propidium iodide (PI) for 15 min at room temperature in the dark. The stained cells were detected using the BD FACSAria II flow cytometer (BD Biosciences, Hercules, CA, USA).

Transwell Invasion Assay

According to the manufacturer's instructions, the invasion assay was performed using Transwell chambers (8 μm pore size; Corning, NY, USA). The cells were transfected with plasmid or siRNA, as described above. After 48 h, the cells were trypsinized and resuspended in serum-free RPMI-1640 medium. 5×10^4 Cells, suspended in 0.5 mL of no FBS media, were plated in the upper chamber with a coated extracellular matrix (ECM) gel (BD Biosciences, Franklin Lakes, NJ, USA) for the invasion assay. RPMI-1640 medium with 10% FBS was added into the lower chamber. After incubation for 24 h, cells that did not invade were mechanically removed with a cotton swab, and the membranes were fixed with 4% paraformalin for 20 min. Then, the cells were stained with crystal violet for 30 min at room temperature. Three different areas of each well were randomly selected for imaging by microscopy (Olympus IX51). Cell numbers were quantified by Image-Pro Plus 6.0 (Media Cybernetics, MD, USA).

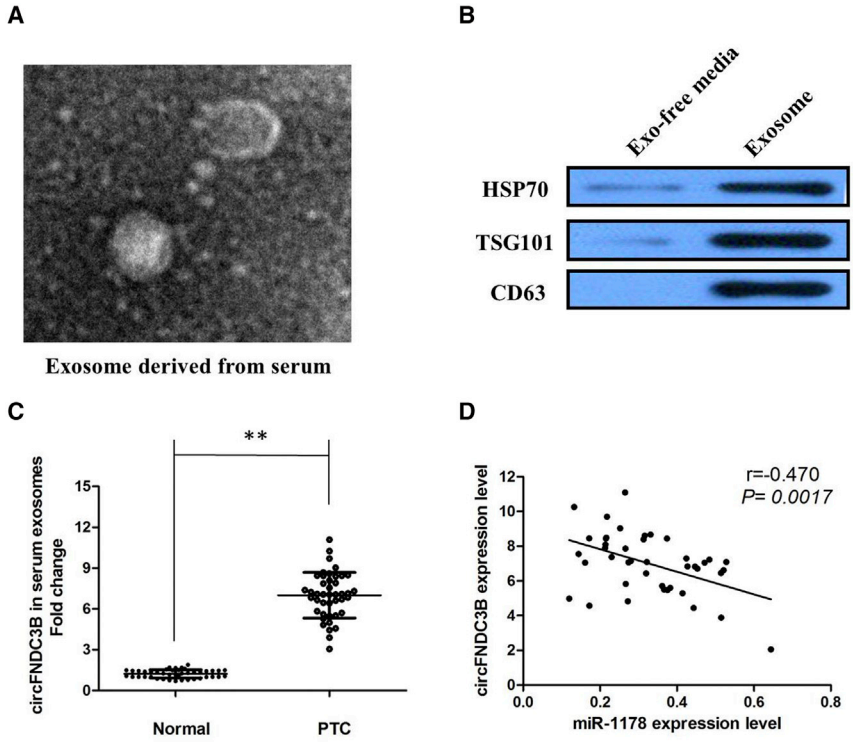

Figure 7. circFNDC3B Is Secreted by Exosomes into Serum of PTC Patients

(A) circFNDC3B was secreted into exosomes derived from serum of PTC patients. A representative image of exosome (indicated by red arrows) derived from serum of PTC patients detected from an electron microscope. (B) Western blot showing the expression of TSG101 and HSP70, which are the markers of exosome from purified serum exosome. (C) qRT-PCR for the abundance of circFNDC3B in serum exosomes. The levels of circFNDC3B in serum exosomes from PTC patients were significantly higher than that in normal individuals. (D) The expression levels of circFNDC3B were negatively correlated with that of miR-1178 in the exosomes extracted from serum of PTC patients. All tests were at least performed three times. Data were expressed as mean ± SD. **$p < 0.01$.

In Vivo Tumorigenicity Assay

sh-circFNDC3B and sh-NC, constructed by GenePharma, were used for the *in vivo* tumorigenicity assay. The sh-circFNDC3B and sh-NC were incorporated into a pLKO vector to produce the pLKO-sh-circFNDC3B and pLKO-sh-NC plasmids. A lentivirus carrying either pLKO-sh-circFNDC3B or pLKO-sh-NC was introduced into cells. To obtain the stable knockdown cell line, the transfected cells were selected with 2 g/mL puromycin. BALB/c nude mice (male, 5 weeks old) were acquired from Beijing Vital River Laboratory Animal Technology, and all mice were raised in a specific pathogen-free environment. All nude mice were randomly classified into either the sh-circFNDC3B or sh-NC group. Mice in the sh-circFNDC3B group were subcutaneously injected with TPC-1 cells stably transfected with pLKO-sh-circFNDC3B, whereas those in the sh-NC group were subcutaneously injected with cells stably transfected with pLKO-sh-NC. Following successful transplantation, tumor width and length were measured every 5 days. All nude mice were sacrificed on day 30, and the tumor xenografts were resected and weighed. The volume of tumor xenografts was calculated using the following formula: (length $\times$ width^2)/2. All experimental steps were approved by the Ethics Committee for Animal Research of Shandong Provincial Hospital Affiliated to Shandong University.

Western Blotting

Total protein was extracted with 1 times NuPAGE LDS Sample Buffer (Thermo Fisher Scientific), according to the manufacturer's instructions. To identify exosome markers, primary antibodies against TLR4, CD63, and TSG101 were purchased from Abcam (Cambridge, UK), and primary antibodies against HSP70 were obtained from Cell Signaling Technology (CST; Beverly, MA, USA). The secondary antibodies were f(ab)2 fragments of donkey anti-mouse immunoglobulin or donkey anti-rabbit immunoglobulin linked to horseradish peroxidase (Jackson ImmunoResearch, USA). Immunoblotting reagents from an electrochemiluminescence kit were used (Amersham Biosciences, Uppsala, Sweden).

Bioinformatic Analysis

Agilent Feature Extraction software (version 11.0.1.1) was used to analyze acquired array images. Data processing was performed using the R software package. Differentially expressed circRNAs with statistical significance between two groups were identified through volcano plot filtering. Differentially expressed circRNAs between two samples were identified through fold-change filtering. The circRNA/microRNA interaction was predicted with ArrayStar's home-made software based on TargetScan and miRanda.

Luciferase Reporter Assay

Fragments of circFNDC3B containing the predicted WT miR-1178 binding site were amplified by GenePharma and inserted into a pmirGLO Dual-Luciferase miRNA Target Expression Vector (Promega, Madison, WI, USA), generating the WT-circFNDC3B reporter plasmid. A mutant (MUT)-circFNDC3B reporter plasmid was designed and produced in a similar manner. For the luciferase reporter assay, the cotransfection of either miR-1178 mimics or miR-NC and either WT-circFNDC3B or MUT-circFNDC3B into PTC cells was performed using Lipofectamine 2000. After culturing for 48 h, luciferase activity was quantified using the Dual-Luciferase Reporter Assay System (Promega). The value of firefly luciferase was normalized to that of Renilla luciferase.

RIP Assay

RIP assay was performed using an EZ-Magna RIP kit (Millipore, Billerica, MA, USA) in accordance with the manufacturer's instructions. Cells were lysed at 70%–80% confluence in RIP lysis buffer and then incubated with magnetic beads conjugated with human anti-AGO2 antibody (Millipore) and normal mouse immunoglobulin G (IgG) control (Millipore) in RIP buffer. The RNAs in the immunoprecipitates were isolated with TRIzol reagent and analyzed by qRT-PCR.

IHC

IHC analysis was performed under the manufacturer's instructions. Briefly, the slides were incubated with primary antibodies overnight at 4°C and then incubated with secondary antibodies at room temperature for 2 h. The expression was evaluated using a composite score obtained by multiplying the values of staining intensities (0, no staining; 1, weak staining; 2, moderate staining; 3, strong staining) and the percentage of positive cells (0, 0%; 1, <10%; 2, 10%–50%; 3, >50%).

Plasma Exosome Isolation

First, the samples were centrifuged twice at 3,000 *g* and 10,000 *g* for 20 min at room temperature to remove cells and other debris in the plasma. The supernatants were then centrifuged at 100,000 *g* for 30 min at 4°C to remove microvesicles that were larger than exosomes, harvested, and again centrifuged at 10,000 *g* for 70 min at 4°C. Subsequently, the supernatants were gently decanted, and the exosome sediments were resuspended in PBS. Concentration of exosomes was determined using the bicinchoninic acid (BCA) method, as recommended by the manufacturer (Thermo Scientific, USA).

TEM

Exosomes were suspended in 100 μL of PBS and were fixed with 5% glutaraldehyde at incubation temperature and then maintained at 4°C until TEM analysis. According to the TEM sample preparation procedure, we placed a drop of exosome sample on a carbon-coated copper grid and immersed it in 2% phosphotungstic acid solution (pH 7.0) for 30 s. The preparations were observed with a transmission electron microscope (Tecnai G^2 Spirit BioTWIN, FEI, USA).

NTA

Briefly, the exosomes were resuspended in PBS and filtered with a syringe filter (Millipore). Then, the samples were diluted until individual nanoparticles could be tracked. The size distribution of the exosomes was evaluated using a NanoSight NS300 instrument (Malvern Instruments, Worcestershire, UK).

Statistical Analysis

Data was presented as mean value ± standard deviation (mean ± SD) in this study. GraphPad Prism 6.0 (La Jolla, CA, USA) was recruited to conduct statistical analysis. Multiple comparisons were conducted by the one-way analysis of variance (ANOVA) test. A p value less than 0.05 was thought to be statistically significant.

SUPPLEMENTAL INFORMATION

Supplemental Information can be found online at https://doi.org/10.1016/j.omtn.2019.12.025.

AUTHOR CONTRIBUTIONS

L.G. and X.T. performed primers design and experiments and wrote the paper. W.Z. and G.W. contributed the flow cytometry assay and animal experiments. X.P. and Z.S. collected and classified the human tissue samples. Y.S. and H.X. contributed to RT-PCR and qRT-PCR. P.S. analyzed the data. All authors read and approved the final manuscript.

CONFLICTS OF INTEREST

The authors declare no competing interests.

ACKNOWLEDGMENTS

The study was approved by the Medical Ethics Committee of Shandong Provincial Hospital Affiliated to Shandong University. We have received consents from individual patients who have participated in this study. The consent forms will be provided upon request. The datasets supporting the conclusions of this article are included within the article and its additional files. This work was supported by the Natural Science Foundation of Shandong Province (ZR2014HM115), Scientific Research Project of Shandong University (12721742), and Key Projects of Jinan Science and Technology Bureau (201805011).

REFERENCES

1. Cabanillas, M.E., McFadden, D.G., and Durante, C. (2016). Thyroid cancer. Lancet *388*, 2783–2795.

2. Kitahara, C.M., and Sosa, J.A. (2016). The changing incidence of thyroid cancer. Nat. Rev. Endocrinol. *12*, 646–653.

3. Li, N., Du, X.L., Reitzel, L.R., Xu, L., and Sturgis, E.M. (2013). Impact of enhanced detection on the increase in thyroid cancer incidence in the United States: review of incidence trends by socioeconomic status within the surveillance, epidemiology, and end results registry, 1980-2008. Thyroid *23*, 103–110.

4. Siegel, R.L., Miller, K.D., and Jemal, A. (2018). Cancer statistics, 2018. CA Cancer J. Clin. *68*, 7–30.

5. Hsu, M.T., and Coca-Prados, M. (1979). Electron microscopic evidence for the circular form of RNA in the cytoplasm of eukaryotic cells. Nature *280*, 339–340.

6. Du, W.W., Fang, L., Yang, W., Wu, N., Awan, F.M., Yang, Z., and Yang, B.B. (2017). Induction of tumor apoptosis through a circular RNA enhancing Foxo3 activity. Cell Death Differ. *24*, 357–370.

7. Zhang, Y., Zhang, X.O., Chen, T., Xiang, J.F., Yin, Q.F., Xing, Y.H., Zhu, S., Yang, L., and Chen, L.L. (2013). Circular intronic long noncoding RNAs. Mol. Cell *51*, 792–806.

8. Ashwal-Fluss, R., Meyer, M., Pamudurti, N.R., Ivanov, A., Bartok, O., Hanan, M., Evantal, N., Memczak, S., Rajewsky, N., and Kadener, S. (2014). circRNA biogenesis competes with pre-mRNA splicing. Mol. Cell *56*, 55–66.

9. Hansen, T.B., Jensen, T.I., Clausen, B.H., Bramsen, J.B., Finsen, B., Damgaard, C.K., and Kjems, J. (2013). Natural RNA circles function as efficient microRNA sponges. Nature *495*, 384–388.

10. Zheng, Q., Bao, C., Guo, W., Li, S., Chen, J., Chen, B., Luo, Y., Lyu, D., Li, Y., Shi, G., et al. (2016). Circular RNA profiling reveals an abundant circHIPK3 that regulates cell growth by sponging multiple miRNAs. Nat. Commun. *7*, 11215.

11. Wei, H., Pan, L., Tao, D., and Li, R. (2018). Circular RNA circZFR contributes to papillary thyroid cancer cell proliferation and invasion by sponging miR-1261 and facilitating C8orf4 expression. Biochem. Biophys. Res. Commun. *503*, 56–61.

12. Wang, M., Chen, B., Ru, Z., and Cong, L. (2018). CircRNA circ-ITCH suppresses papillary thyroid cancer progression through miR-22-3p/CBL/β-catenin pathway. Biochem. Biophys. Res. Commun. *504*, 283–288.

13. Cai, X., Zhao, Z., Dong, J., Lv, Q., Yun, B., Liu, J., Shen, Y., Kang, J., and Li, J. (2019). Circular RNA circBACH2 plays a role in papillary thyroid carcinoma by sponging miR-139-5p and regulating LMO4 expression. Cell Death Dis. *10*, 184.

14. Liu, H., Bi, J., Dong, W., Yang, M., Shi, J., Jiang, N., Lin, T., and Huang, J. (2018). Invasion-related circular RNA circFNDC3B inhibits bladder cancer progression through the miR-1178-3p/G3BP2/SRC/FAK axis. Mol. Cancer *17*, 161.

15. Hong, Y., Qin, H., Li, Y., Zhang, Y., Zhuang, X., Liu, L., Lu, K., Li, L., Deng, X., Liu, F., et al. (2019). FNDC3B circular RNA promotes the migration and invasion of gastric cancer cells via the regulation of E-cadherin and CD44 expression. J. Cell. Physiol. *234*, 19895–19910.

16. Keller, S., Sanderson, M.P., Stoeck, A., and Altevogt, P. (2006). Exosomes: from biogenesis and secretion to biological function. Immunol. Lett. *107*, 102–108.

17. van der Pol, E., Böing, A.N., Harrison, P., Sturk, A., and Nieuwland, R. (2012). Classification, functions, and clinical relevance of extracellular vesicles. Pharmacol. Rev. *64*, 676–705.

18. Tang, W., Fu, K., Sun, H., Rong, D., Wang, H., and Cao, H. (2018). CircRNA microarray profiling identifies a novel circulating biomarker for detection of gastric cancer. Mol. Cancer *17*, 137.

19. Li, S., Li, Y., Chen, B., Zhao, J., Yu, S., Tang, Y., Zheng, Q., Li, Y., Wang, P., He, X., and Huang, S. (2018). exoRBase: a database of circRNA, lncRNA and mRNA in human blood exosomes. Nucleic Acids Res. *46* (D1), D106–D112.

20. Dai, X., Chen, C., Yang, Q., Xue, J., Chen, X., Sun, B., Luo, F., Liu, X., Xiao, T., Xu, H., et al. (2018). Exosomal circRNA_100284 from arsenite-transformed cells, via microRNA-217 regulation of EZH2, is involved in the malignant transformation of human hepatic cells by accelerating the cell cycle and promoting cell proliferation. Cell Death Dis. *9*, 454.

21. Wang, H., Yan, X., Zhang, H., and Zhan, X. (2019). CircRNA circ_0067934 Overexpression Correlates with Poor Prognosis and Promotes Thyroid Carcinoma Progression. Med. Sci. Monit. *25*, 1342–1349.

22. Pan, Y., Xu, T., Liu, Y., Li, W., and Zhang, W. (2019). Upregulated circular RNA circ_0025033 promotes papillary thyroid cancer cell proliferation and invasion via sponging miR-1231 and miR-1304. Biochem. Biophys. Res. Commun. *510*, 334–338.

23. Liu, F., Zhang, J., Qin, L., Yang, Z., Xiong, J., Zhang, Y., Li, R., Li, S., Wang, H., Yu, B., et al. (2018). Circular RNA EIF6 (Hsa_circ_0060060) sponges miR-144-3p to promote the cisplatin-resistance of human thyroid carcinoma cells by autophagy regulation. Aging (Albany N.Y.) *10*, 3806–3820.

24. Garikipati, V.N.S., Verma, S.K., Cheng, Z., Liang, D., Truongcao, M.M., Cimini, M., Yue, Y., Huang, G., Wang, C., Benedict, C., et al. (2019). Circular RNA CircFndc3b modulates cardiac repair after myocardial infarction via FUS/VEGF-A axis. Nat. Commun. *10*, 4317.

25. Hu, W., Bi, Z.-Y., Chen, Z.-L., Liu, C., Li, L.-L., Zhang, F., Zhou, Q., Zhu, W., Song, Y.-Y.-Y., Zhan, B.-T., et al. (2018). Emerging landscape of circular RNAs in lung cancer. Cancer Lett. *427*, 18–27.

26. Han, D., Li, J., Wang, H., Su, X., Hou, J., Gu, Y., Qian, C., Lin, Y., Liu, X., Huang, M., et al. (2017). Circular RNA circMTO1 acts as the sponge of microRNA-9 to suppress hepatocellular carcinoma progression. Hepatology *66*, 1151–1164.

27. Hsiao, K.Y., Lin, Y.C., Gupta, S.K., Chang, N., Yen, L., Sun, H.S., and Tsai, S.J. (2017). Noncoding effects of circular RNA CCDC66 promote colon cancer growth and metastasis. Cancer Res. *77*, 2339–2350.

28. Salmena, L., Poliseno, L., Tay, Y., Kats, L., and Pandolfi, P.P. (2011). A ceRNA hypothesis: the Rosetta Stone of a hidden RNA language? Cell *146*, 353–358.

29. Su, H., Tao, T., Yang, Z., Kang, X., Zhang, X., Kang, D., Wu, S., and Li, C. (2019). Circular RNA cTFRC acts as the sponge of MicroRNA-107 to promote bladder carcinoma progression. Mol. Cancer *18*, 27.

30. Yang, R., Xing, L., Zheng, X., Sun, Y., Wang, X., and Chen, J. (2019). The circRNA circAGFG1 acts as a sponge of miR-195-5p to promote triple-negative breast cancer progression through regulating CCNE1 expression. Mol. Cancer *18*, 4.

31. Ambros, V. (2004). The functions of animal microRNAs. Nature *431*, 350–355.

32. Thakur, B.K., Zhang, H., Becker, A., Matei, I., Huang, Y., Costa-Silva, B., Zheng, Y., Hoshino, A., Brazier, H., Xiang, J., et al. (2014). Double-stranded DNA in exosomes: a novel biomarker in cancer detection. Cell Res. *24*, 766–769.

OMTN, Volume *19*

Supplemental Information

Circular RNA Profiling Reveals Exosomal circ_0006156 as a Novel Biomarker in Papillary Thyroid Cancer

Guojun Wu, Wenhong Zhou, Xiaohua Pan, Zhigang Sun, Yongjie Sun, Hao Xu, Peng Shi, Jiyu Li, Ling Gao, and Xingsong Tian

miRNA Predictions

CircRNA Mirbase ID	CircRNA (Top) - miRNA (Bottom) pairing	TargetScan miRNA pr Site Type	 CircRN A Start
hsa_circ_0006156 (5' ... 3') hsa-miR-1178 (3' ... 5')	CCCACACAAUAUAUGGUGAGCAA ||||||| GAUCCCUUCUUGUCACUCGUU	8mer-1a	236
hsa_circ_0006156 (5' ... 3') hsa-miR-1181 (3' ... 5')	AAUUAAGAAAACAGAGCGACGAG |||||| GCCGAGCCCACCGCCGCUGCC	7mer-1a	480
hsa_circ_0006156 (5' ... 3') hsa-miR-1281 (3' ... 5')	AGUGGUGGAAGUGGCGGAGGCGG ||| ||||||| CCCUCUCCU-CCUCCGCU	7mer-m8	439
hsa_circ_0006156 (5' ... 3') hsa-miR-1298 (3' ... 5')	GAAGCAGCCCAAAGUCGAAUGAU ||||||| AUGUAGACCUGUCGGCUUACUU	7mer-m8	506

hsa_circ_0006156 (5' ... 3') hsa-miR-1304 (3' ... 5')	UCGAUCGCCAGAACCGCCUCAAC ||||||| GUGUAGAGUGACAUCGGAGUUU	7mer-m8	350
hsa_circ_0006156 (5' ... 3') hsa-miR-1322 (3' ... 5')	UCAGUUUUUUCCCCAGCAUCAUC ||||||| GUCGUAGUCGUCGUAGUAG	7mer-m8	210
hsa_circ_0006156 (5' ... 3') hsa-miR-147b (3' ... 5')	CAGUACAGCAAGCCU--CCGCACAA |||| ||||||| AUCGUCUUCGUAAAGGCGUGUG	8mer-1a	307
hsa_circ_0006156 (5' ... 3') hsa-miR-194 (3' ... 5')	CGGCUUACUACCCACCUGUUACC ||||||| AGGUGUACCUCAACGACAAUGU	7mer-m8	167
hsa_circ_0006156 (5' ... 3') hsa-miR-210 (3' ... 5')	AGUACAGCAAGCCUCCGCACAAA |||||| AGUCGGCGACAGUGUGCGUGUC	7mer-1a	308

hsa_circ_0006156 (5’ ... 3’) hsa-miR-510 (3’ ... 5’)	GUCACACCCCAGUCUCCUGAGUG ||| ||||||| CACUAACGGUGAGAGGACUCAU	7mer-m8	52
hsa_circ_0006156 (5’ ... 3’) hsa-miR-568 (3’ ... 5’)	GCAGCUGCACAACAGUAUACAAU |||||| CACACAUAUGUAAAUAUGUA	7mer-1a	398
hsa_circ_0006156 (5’ ... 3’) hsa-miR-578 (3’ ... 5’)	ACAAUAUAUGGUGAGCAAGAAAU |||||| UGUUAGGAUCUCGUGUUCUUC	7mer-1a	241
hsa_circ_0006156 (5’ ... 3’) hsa-miR-587 (3’ ... 5’)	GAAAUUAUACCAUUU--UAUGGAAU ||| ||||||| CACUGAGUAGUGGAUACCUUU	7mer-m8	259
hsa_circ_0006156 (5’ ... 3’) hsa-miR-1270 (3’ ... 5’)	UACCCCUCAGCCAUGUCUCCAAC |||||| UGUGUCGAGAAGGUAUAGAGGUC	7mer-1a	88

hsa_circ_0006156 (5' ... 3') hsa-miR-620 (3' ... 5')	UACCCCUCAGCCAUGUCUCCAAC |||||| UAAAGAUAUAGAUAGAGGUA	7mer-1a	88
hsa_circ_0006156 (5' ... 3') hsa-miR-625 (3' ... 5')	GUCUCCUGAGUGUUAUCCCCCAA |||||| CCUGAUAUCUUGAAAGGGGGA	7mer-1a	63
hsa_circ_0006156 (5' ... 3') hsa-miR-644 (3' ... 5')	CCAGCAUCAUCUUCCCCACACAA |||||| CGAGAUUCUUUCGGUGUGA	7mer-1a	222
hsa_circ_0006156 (5' ... 3') hsa-miR-658 (3' ... 5')	GACCAGUACAGCAAGCCUCCGCA ||||||| UGGUUGCCUGGAUGAAGGGAGGCGG	8mer-1a	304
hsa_circ_0006156 (5' ... 3') hsa-miR-766 (3' ... 5')	CACCUGUUACCGGACCUGGAGAU |||||| CGACUCCGACACCCCGACCUCA	7mer-1a	179

hsa_circ_0006156 (5' ... 3') hsa-miR-941 (3' ... 5')	AUAGUACUGGAGUCCGCCGGGUG ||||||| CGUGUACACGUGUGUCGGCCCAC	7mer-m8	26
hsa_circ_0006156 (5' ... 3') hsa-miR-942 (3' ... 5')	CAACCUACAUCACCCGAGAAGAC |||||| GUGUACCGGUUUUGUCUCUUCU	7mer-1a	284

edictions							
CircRNA End	3' pairing	local AU	position	TA	SPS	context + score	context + score percentile
243	0.003	-0.01	-0.055	0	-0.068	-0.377	99
486	0.015	0.025	-0.046	-0.149	-0.068	-0.297	64
445	-0.016	0.101	-0.05	-0.042	-0.101	-0.228	86
512	0.021	-0.025	-0.06	-0.004	0.031	-0.157	98

356	0.003	0.074	-0.038	0.001	-0.034	-0.114	85
216	0.003	0.012	-0.032	-0.017	0.009	-0.145	91
314	-0.039	0.005	-0.06	-0.128	-0.112	-0.581	99
173	0.021	0.082	-0.038	0	0.027	-0.028	75
314	0.001	0.005	-0.027	-0.072	-0.046	-0.213	84

58	-0.016	0.022	-0.054	0.003	-0.033	-0.198	95
404	0.004	0.015	-0.037	0.004	0.059	-0.029	86
247	-0.002	-0.023	-0.024	0.017	0.042	-0.064	85
265	-0.016	-0.059	-0.025	0.023	0.043	-0.154	96
94	-0.002	0.038	-0.04	0.006	-0.034	-0.106	84

94	0.001	0.038	-0.04	0.006	-0.034	-0.103	83
69	0.001	0.019	-0.043	0.021	-0.118	-0.194	91
228	0.004	-0.012	-0.026	0.002	-0.05	-0.156	87
311	0.003	0.036	-0.06	-0.07	-0.172	-0.51	98
185	-0.002	0.019	-0.031	0.031	-0.048	-0.105	79

32	0.003	0.085	-0.058	-0.07	-0.114	-0.274	86
290	0.001	0.037	-0.024	0.023	0	-0.037	70